Beyond Classical Theory: Predicting the Free Energy Barrier of Bubble Nucleation in Polymer Foaming

Isamu Kusaka
William G. Lowrie Dept. of Chemical and Biomolecular Engineering, The Koffolt Laboratories, The Ohio State University, Columbus, OH 43210

Manish Talreja
School of Chemical and Biomolecular Engineering, Georgia Institute of Technology, NW, Atlanta, GA 30332

David L. Tomasko
William G. Lowrie Dept. of Chemical and Biomolecular Engineering, The Koffolt Laboratories, The Ohio State University, Columbus, OH 43210

DOI 10.1002/aic.14062
Published online March 4, 2013 in Wiley Online Library (wileyonlinelibrary.com)

Based on the Gibbs-Tolman-Koenig formalism, we considered the Tolman correction to the free energy barrier of bubble nucleation in polymer-gas binary mixtures. For this class of systems, the correction may be estimated with a reasonable accuracy using experimentally accessible macroscopic thermodynamic quantities only. Although the Tolman correction is applicable only in the low supersaturation regime, a simple ansatz regarding the supersaturation dependence of the Tolman length can be made to extend the usefulness of this approach and to yield the free energy barrier that vanishes at the mean-field spinodal as demanded by thermodynamic considerations. © 2013 American Institute of Chemical Engineers *AIChE J*, 59: 3042–3053, 2013
Keywords: bubble nucleation, polymer foam, Tolman length

Introduction

A precise control of bubble nucleation in polymer-gas system is crucial in producing light-weight and high-strength plastic foams as structural components in applications such as automobiles and wind turbines. Their mechanical properties depend strongly on the cell density and structure, which in turn are controlled by nucleation.[1,2] In insulating materials, the insulating property again depends on such morphological characteristics. Yet, the plastic foam industry currently faces a significant challenge in continuing to produce high quality foams as the traditional physical blowing agents, such as chlorofluorocarbons and hydrochlorofluorocarbons are being phased out due to their undesirable environmental impacts.[3] Environmentally benign carbon dioxide has emerged as a promising alternative. However, a fundamental understanding of bubble nucleation in polymer-CO_2 system is needed to minimize trial and error and shift quickly to the processes using this alternative blowing agent.

Thus far, so-called classical theory[4] has been used as the primary source of theoretical guidance in understanding nucleation processes. However, the theory is often inadequate as a predictive tool. In fact, its prediction of the rate of nucleation can be easily off by many orders of magnitude. This failure of classical theory is a result of its inability to predict accurately the free energy barrier of nucleation, that is, formation of a critical nucleus. In particular, the theory does not incorporate the dependence of the interfacial tension, a key quantity in computing the free energy barrier, on the size of the critical nucleus.

This dependence can, in principle, be predicted by means of the Gibbs-Tolman-Koenig (GTK) aic14062-math-,[5–8] provided that the so-called Tolman length is known as a function of supersaturation. In general, however, this requires costly statistical mechanical calculations.[9–14] In fact, the Tolman length of a critical nucleus is not any more accessible to an experimental measurement than its interfacial tension is. Thus, the entire formalism simply transfers the difficulty of measuring the latter to that of measuring the former.

Nevertheless, the alternative formulation by means of the GTK equation can lead to new ways of introducing potentially useful approximations that are not readily obvious otherwise. In fact, some efforts in this direction have been reported for single-component systems.[15,16] In this article, we focus on the case of bubble nucleation in polymer-gas mixtures and present an approximation, in which the Tolman length, in the low supersaturation limit, is evaluated using macroscopically accessible thermodynamic properties only. The accuracy of the approximation is examined by comparing its predictions against the Monte Carlo simulation of a simple model system of polymer-CO_2 mixtures. To integrate the GTK equation beyond the low supersaturation regime, we also consider a simple ansatz relating the Tolman length

Correspondence concerning this article should be addressed to I. Kusaka at kusaka.2@osu.edu.
Current address of Manish Talreja: The Dow Chemical Company, 727 Norristown Road, Spring House, PA 19477.

to the degree of supersaturation. Unlike classical theory, the resulting free energy barrier agrees with the Tolman correction in the low supersaturation regime and vanishes at the onset of the mean-field spinodal as demanded by thermodynamic considerations.

Classical Nucleation Theory

Relaxation of a metastable phase toward a more stable one accompanies nucleation, in which a small fragment of the new phase forms in the matrix of the metastable phase. The steady-state nucleation rate J, that is, the number of such fragments of the critical size that are being created per unit time and unit volume, is given by[4]

$$J = J_k e^{-W/k_B T} \tag{1}$$

where W, k_B, T, and J_k are, respectively, the free energy required to form a critical nucleus in the metastable phase, the Boltzmann constant, the absolute temperature, and a constant determined by kinetic considerations.

As W appears in the exponent, an accurate evaluation of W is expected to be more important than that of J_k. A formally exact expression for W was obtained by Gibbs[17] and is given by

$$W = \frac{16\pi\gamma^3}{3(\Delta p)^2} \tag{2}$$

where γ is the surface tension and $\Delta p := p^\beta - p^\alpha$, wherein p^α is the pressure of the metastable phase, and p^β is the pressure the nucleating phase would have if it were present in bulk (without any interfaces) and held at the same temperature and chemical potentials as the metastable phase.

In the case of bubble nucleation from a metastable binary polymer-gas liquid mixture, the polymer molecules may be considered to be absent from the bulk gas phase, and p^β is determined by the equality of temperature and that of the chemical potential of the gas species only

$$\mu_g^\alpha\left(T, p^\alpha, x_g\right) = \mu_g^\beta\left(T, p^\beta\right) \tag{3}$$

where the subscript g refers to the gas species. The mole fraction x_g of the mixture is denoted without the superscript α because the corresponding value in β phase is always unity. We note that, as a nucleus becomes small, p^β determined by Eq. 3 starts to deviate significantly from the pressure realized at its center. Nevertheless, Eq. 2 with p^β so determined remains valid even for a vanishingly small critical nucleus as long as the nucleus is spherically symmetric.[17,18]

The difficulty in applying Eq. 2 lies in the fact that γ of a critical nucleus is not directly measurable. Classical theory, thus, replaces γ by γ_∞, the surface tension of the macroscopic interface observed at saturation, and estimates W as

$$W^{cl} = \frac{16\pi\gamma_\infty^3}{3(\Delta p)^2} \tag{4}$$

However, W^{cl} starts to deviate significantly from the true value W with increasing supersaturation. A thermodynamic consideration demands that γ, R, and W vanish simultaneously at the mean-field spinodal,[17] whereas W^{cl} does not. Moreover, Δp is often explained incorrectly in the literature as the applied pressure drop to induce bubble nucleation. This misconception causes Δp to be overestimated, leading to an overprediction of the nucleation rate.[3] In contrast, the error arising from the use of γ_∞ instead of γ can lead to a serious under prediction of the rate. Even though these two sources of error tend to cancel each other to some extent, it would not be satisfactory to advance a theory that relies on such fortuitous cancellation of errors.

Theory

Classical theory, despite its shortcomings, is still very attractive because the value of W^{cl} can be estimated using thermodynamic properties accessible to macroscopic measurements. In fact, equations of state of the bulk phases involved yield Δp by means of Eq. 3, whereas γ_∞ can be measured by a mechanical means, though only with a considerable difficulty in certain cases.[19] It is then at least tempting to seek for ways to correct W^{cl} rather than to evaluate W *ab initio* without referring to classical theory. This will be a sensible approach if, as was indicated by density functional studies of simple fluids,[20,21] the system-specific part of W is contained mostly in W^{cl} and the correction, in the form of $\left(W - W^{cl}\right)/W^{cl}$, turns out to be rather generic across various systems.

Because both W and W^{cl} tend toward infinity as the supersaturation is reduced, it is convenient to consider the ratio $\phi := W/W^{cl} = (\gamma/\gamma_\infty)^3$ or, more simply,

$$\psi := \frac{\gamma}{\gamma_\infty} \tag{5}$$

both of which are unity at saturation, vanish at the mean-field spinodal, and remain positive and finite between these two limiting cases. With these definitions, the problem of computing W is equivalent to that of determining φ (or ψ) as a function of the degree of supersaturation.

Supersaturation

To begin our formulation, we need to choose a quantitative measure of supersaturation. As the intensive state of the metastable phase α may be specified by $\left(T, p^\alpha, x_g\right)$, a change in any of these variables results in a change in the degree of supersaturation. In polymer foaming, however, supersaturation is commonly achieved by first saturating the polymer with gas under some initial pressure p_i and then dropping the pressure suddenly to some final pressure p_f.

If the nucleation occurs sufficiently slowly compared to the time scale required for the system to establish mechanical equilibrium under the new pressure p_f, we may regard the nucleation to be taking place at p_f. This allows us to identify p_f with p^α. (In what follows, therefore, $p_f \equiv p^\alpha$ and we shall refer mostly to p^α.) On the other hand, x_g will not change significantly from its initial value that is determined at T and p_i until later in the bubble growth stage.

The statistical behavior, such as J, of the metastable phase, being at a state of equilibrium, is independent of the history that brought about the metastability. Accordingly, a given metastable phase may be regarded as being on a path of increasing x_g (achieved by increasing p_i) for given values of T and p^α as indicated by path A in Figure 1. This same metastable phase may also be regarded as being on a path of decreasing p^α at given T and p_i (and hence x_g) as indicated by path B in Figure 1.

As seen from Figure 1, the appropriate choice for the state of saturation, and hence the value of γ_∞ to be used in Eq. 5, depend on the path being chosen. Using the superscripts A

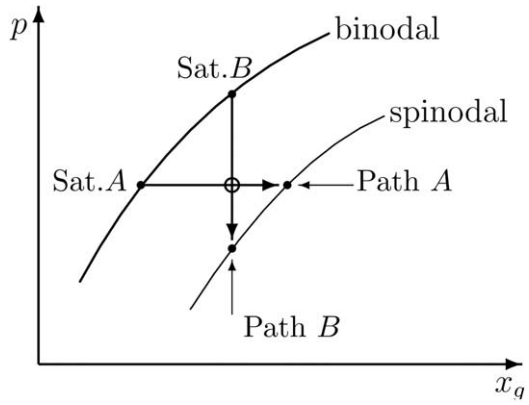

Figure 1. Two paths of increasing supersaturation.

A given metastable state, represented by an open circle, can be analyzed from two distinct points of view, that is, as being on the path of increasing x_g or the one of decreasing p^α. Sat. *A* and Sat. *B* refer to the appropriate choice for the state of saturation for paths *A* and *B*, respectively.

and B to denote the two paths considered above, $\psi^A \neq \psi^B$ for a given metastable state. This distinction between the two paths, however, is actually one of perspective and reflects one's choice on how the set of experiments, performed at various values of x_g and p^α, is going to be analyzed.

Although x_g or p^α, depending on the path taken, serves as a quantitative measure of supersaturation, it is more convenient to use Δp instead. This is possible because the set of variables (T, p^α, x_g), through Eq. 3, completely determines the intensive state of the bulk β phase including p^β and because Δp is expected to change monotonically when x_g (or p^α) alone is varied while holding constant the remaining two variables T and p^α (or x_g).

To summarize, we take

$$(T, p^\alpha, \Delta p) \tag{6}$$

for path A and

$$(T, \Delta p, x_g) \tag{7}$$

for path B as the set of independent variables specifying the intensive state of the metastable phase. In both cases, Δp quantifies the degree of supersaturation and, starting from zero at saturation, increases monotonically until the onset of the mean-field spinodal is reached. We note that Δp stays finite throughout.

Supersaturation dependence of ψ

Our starting point is the following differential equation

$$\frac{\partial \psi}{\partial \Delta p} = \frac{1}{\gamma_\infty}\frac{\partial \gamma}{\partial \Delta p} = -\frac{\delta}{\gamma_\infty}\left(1 + \delta q + \frac{1}{3}\delta^2 q^2\right) \tag{8}$$

where q is the curvature of the surface of tension and δ is the Tolman length defined as the distance between the surface of tension and the auxiliary dividing surface to be specified shortly. Equation 8 is a form of the GTK equation[5–8] and is derived in Appendix A specifically for the case of bubble nucleation in polymer-gas binary mixtures.

Equation 8 applies to both path A and path B. The distinction between the paths lies in the set of variables to be held fixed in evaluating the partial derivatives and in the definition of the auxiliary surface. Thus, T and p^α are held fixed for path A, whereas x_g in place of p^α is held fixed for path B.

For path A, the location of the auxiliary surface is determined so that

$$x_g \Gamma_{p,a} - x_p \Gamma_{g,a} = 0 \tag{9}$$

holds. Here, $x_p = 1 - x_g$ is the mole fraction of polymer and $\Gamma_{i,a}$ is the excess number of molecules of species i, attributed to the unit area of the auxiliary surface. The subscript a signifies that the surface excess quantities are defined with respect to the auxiliary surface. For path B, Eq. 9 must be replaced by

$$V_g^\alpha \Gamma_{g,a} + V_p^\alpha \Gamma_{p,a} = 0 \tag{10}$$

where V_i^α is the partial molar volume of species i in the polymer-gas mixture.

At saturation, where $\Delta p = 0$, $q = 0$, and $\gamma = \gamma_\infty$, Eq. 8 reduces to

$$\left.\frac{\partial \psi}{\partial \Delta p}\right|_{\Delta p = 0} = -\frac{\delta_\infty}{\gamma_\infty} \tag{11}$$

where δ_∞ is the value of δ at saturation. According to Eq. A13, δ_∞ is positive if the auxiliary surface penetrates deeper into the polymer-gas mixture phase than does the surface of tension.

We note that, for path A, the state at which δ_∞ and γ_∞ are to be evaluated refers to the system at saturation at given T and p^α, that is, at the state indicated by the label "Sat. A" in Figure 1. For path B, these quantities must be evaluated at "Sat. B" in Figure 1.

Approximation for δ_∞

As shown by Gibbs,[22] the surface of tension lies within the interfacial region. We expect that the same holds for the equimolar dividing surface defined with respect to polymer ($\Gamma_{p,e}=0$). Thus, for a flat interface, the distance δ_∞ between the auxiliary surface (at z_a) and the surface of tension (at z_s) may be approximated by that between z_a and the equimolar dividing surface (at z_e)

$$\delta_\infty = z_a - z_s = z_a - z_e - (z_s - z_e) \approx z_a - z_e \tag{12}$$

provided that $|z_s - z_e| \ll |z_a - z_e|$.

The virtue of this approximation lies in the fact that the right hand side of Eq. 12 may be estimated for systems of experimental interest using experimentally accessible quantities only. This is demonstrated in Appendix B with the result that

$$\delta_\infty^A \approx v^\beta \Gamma_{g,e} = -\left(\frac{\partial \gamma_\infty}{\partial p^\beta}\right)_T \tag{13}$$

for path A and that

$$\delta_\infty^B \approx -\frac{V_g^\alpha}{V_g^\alpha - v^\beta}\left(\frac{\partial \gamma_\infty}{\partial p^\beta}\right)_T \tag{14}$$

for path B. In these equations, v^β is the volume of phase β defined on the per molecule basis and $\Gamma_{g,e}$ is the surface excess number of gas molecules defined per unit area of the equimolar dividing surface ($\Gamma_{p,e}=0$).

We note that $\left(\partial \gamma_\infty / \partial p^\beta\right)_T$ can be estimated from the measurement of γ_∞ carried out at various values of p^β. Other quantities on the right hand side of Eq. 14 are all accessible to macroscopic measurements.

We must still assess the accuracy of the approximation. Our Monte Carlo simulation study to be presented in a later section indicates that, at least for the range of conditions we explored, the approximation is acceptable for path A but not for path B.

Low supersaturation regime

With approximation Eq. 12, the free energy barrier W in the low supersaturation regime can now be estimated entirely within the confines of macroscopic thermodynamics. To see this, we first recall the familiar Laplace equation

$$\Delta p := p^{\beta} - p^{\alpha} = 2\gamma q \tag{15}$$

expressing the condition of mechanical equilibrium of a critical nucleus and rewrite Eq. 8 as

$$\frac{\partial \psi}{\partial \Delta p} = -\frac{\delta}{\gamma_\infty}\left[1 + \left(\frac{\delta \Delta p}{2\gamma}\right) + \frac{1}{3}\left(\frac{\delta \Delta p}{2\gamma}\right)^2\right] \tag{16}$$

Following Tolman,[7] let us confine our attention to the vicinity of saturation and write

$$\frac{\partial \psi}{\partial \Delta p} = -\frac{\delta_\infty}{\gamma_\infty} + \mathcal{O}(\Delta p) \tag{17}$$

This equation can be readily integrated with the boundary condition that $\psi = 1$ at $\Delta p = 0$ to yield

$$\psi \approx 1 - \eta \tag{18}$$

in which

$$\eta := \frac{\delta_\infty}{\gamma_\infty}\Delta p \tag{19}$$

is a dimensionless measure of the degree of supersaturation. It follows that

$$W = W^{cl}\phi = W^{cl}\psi^3 \approx W^{cl}(1-\eta)^3 \tag{20}$$

Substituting Eq. 15 in Eq. 18 and solving the resulting equation for ψ, we find

$$\psi \approx \frac{1}{1 + 2\delta_\infty q} \tag{21}$$

Written in this way, Eq. 18 is nothing but the famous Tolman correction.

Thermodynamic consistency

To find W over the entire range of supersaturation, δ must be known as a function of q. Only then, the GTK equation can be integrated. In general, however, evaluation of δ requires a costly statistical mechanical study of a system containing a critical nucleus.[9–12,14] In such a study, it is often much easier to find W directly.

A modest advance can still be made while limiting our knowledge only to experimentally accessible macroscopic quantities. We believe that such a line of inquiry is not without a merit especially when it is desirable to circumvent the use of molecular theories either because it is very costly computationally or because the complexity of the system of interest precludes its accurate model representation for statistical mechanical studies.

We first note that Eq. 18 makes a definite prediction regarding the onset of the mean-field spinodal, where γ and hence ψ vanish. In particular, Δp takes the value

$$\Delta p_{sp} \approx \frac{\gamma_\infty}{\delta_\infty} \tag{22}$$

at the onset. Insofar as the mean-field spinodal lies far away from the intended range of applicability of the approximate relation Eq. 18, it is unlikely that Eq. 22 gives a particularly accurate prediction of Δp_{sp}.

However, Tolman's approximation can be modified to ensure the vanishing of ψ at the actual onset of the mean field spinodal, which can be determined using the equation of state of the bulk phase α. For example, one could first assume a simple functional dependence of δ on supersaturation and adjust the parameter(s) in it to ensure the thermodynamic consistency, that is, the simultaneous vanishing of W, γ, and R at the onset. This thermodynamic consistency condition has been invoked in other approaches to determine the supersaturation dependence of the function φ without resorting to molecular theories.[23–25]

As one of the simplest ansatz one can consider, let us suppose that

$$\delta = \delta_\infty \psi^\lambda \tag{23}$$

which clearly satisfies the boundary condition at saturation, where $\psi = 1$. This ansatz can be brought into Eq. 16 to give

$$\frac{\partial \psi}{\partial \eta} = -\psi^\lambda\left[1 + \frac{1}{2}\psi^{\lambda-1}\eta + \frac{1}{3}\left(\frac{1}{2}\psi^{\lambda-1}\eta\right)^2\right] \tag{24}$$

For a given value of λ, Eq. 24 can readily be integrated (numerically) with the boundary condition that $\psi = 1$ at $\eta = 0$. For a positive value of δ_∞, η increases with Δp. One can easily verify that the right hand side of Eq. 24 is negative for any positive value of ψ. Thus, ψ eventually becomes zero at some value of η, which we identify with the onset of the mean-field spinodal and denote by η_{sp}. Because η_{sp} is completely determined by λ, the single parameter λ in our ansatz can be tuned to enforce the thermodynamic consistency.

In contrast, when δ_∞ is negative, η decreases and becomes more negative with increasing supersaturation. As the right hand side of Eq. 24 remains negative in this case also, ψ will keep on increasing with increasing supersaturation (decreasing η). Thus, if δ_∞ is negative, the ansatz Eq. 23 is clearly unacceptable regardless of the value of λ.

As shown in the next section, however, the approximation in Eq. 12 proves accurate only for path A and, for this path, δ_∞ is positive for all conditions we examined. Accordingly, we will continue our discussion with Eq. 23 and explore its consequence in what follows.

To find η_{sp}, we integrated Eq. 24 numerically for various values of λ. As η_{sp} is unknown, it proved convenient to treat ψ and η as the independent and dependent variables, respectively. Then, the integration proceeded from $\psi = 1$ (at which $\eta = 0$) to $\psi = 10^{-14}$ using the Runge–Kutta algorithm with adaptive step size.[26] The value of η at this endpoint was identified with η_{sp}.

The result is shown in Figure 2, which allows λ to be determined once Δp_{sp}, γ_∞, δ_∞, and hence η_{sp} are known. Figure 2 suggests that η_{sp} might diverge as λ approaches unity. As shown in Appendix C, a thermodynamic consideration indeed demands that λ be less than unity.

In passing, we note that, for $\lambda = 0.5$, the numerical solution of Eq. 24 is nearly identical to Eq. 18. Thus, Tolman's approximation, that is, $\lambda = 0$ and truncation at $\mathcal{O}(\Delta p)$, corresponds to $\lambda = 0.5$ but without any truncation. Any solution following from Eq. 24 is consistent with the Tolman correction Eq. 18 in the low supersaturation regime as can be seen by setting $\psi = 1$ and $\eta = 0$ in the equation.

Monte Carlo Simulation

To evaluate the magnitude of δ_∞ and assess the accuracy of the approximation introduced in Eq. 12, Monte Carlo

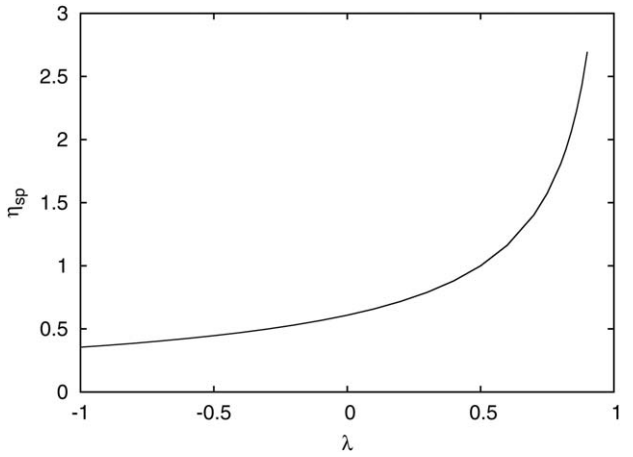

Figure 2. Dependence of the onset of spinodal η_{sp} on the parameter λ in the ansatz Eq. 23.

simulation was carried out for a simple model system of polymer-CO_2 binary mixtures.

Model representation of polymer-CO_2 mixture

We model a polymer chain by n identical spherical segments linearly connected by harmonic springs. Segments are otherwise free to rotate around each other. A CO_2 molecule is modeled as a spherical particle. Interaction between the particles not connected by the harmonic spring is given by the truncated and shifted Lennard–Jones potential

$$\phi_{ij}(r)=\begin{cases}\phi_{ij}^{LJ}(r)-\phi_{ij}^{LJ}\left(R_{ij}^{cut}\right) & (r\le r_c)\\ 0 & (\text{otherwise})\end{cases} \tag{25}$$

in which

$$\phi_{ij}^{LJ}=4\epsilon_{ij}\left[\left(\frac{\sigma_{ij}}{r}\right)^{12}-\left(\frac{\sigma_{ij}}{r}\right)^{6}\right] \tag{26}$$

and $R_{ij}^{cut}=2.5\sigma_{ij}$. The subscript i and j refer either to the spherical particle representing CO_2 or a segment in the chain according to the subscript being g or p.

In reduced units, in which ϵ_{pp} and σ_{pp} are both unity, the natural length of the spring was set to unity while the spring constant was set somewhat arbitrarily to 800, which was neither too soft to allow a pair of connected segments to be separated too far nor too stiff to render a trial translation of a randomly selected segment impractically inefficient. In addition to the usual trial translation of particles, the polymer chains were subjected to configuration bias Monte Carlo moves[27] in which a few segments toward each end of a chain were removed and regrown either on the same or on the opposite end of the remaining chain.

The values of the parameters ϵ_{ij} and σ_{ij} are adjusted so as to reproduce experimentally determined pure component critical temperatures and pressures of CO_2 and octacosane (C_{28}) as well as the experimental solubility data of CO_2 in C_{28}.[28] For the cross-species interaction, we set $\sigma_{gp}=\left(\sigma_{gg}+\sigma_{pp}\right)/2$ and adjusted ϵ_{gp} only.

Using Gibbs ensemble simulation of the pure systems, the critical temperature and pressure were estimated. In terms of reduced units in which ϵ_{ii} and σ_{ii} are both unity, they were, respectively, 1.072 and 0.0934 for CO_2 and 2.136 and 0.00957 for C_{28}, which was represented by a 10 segment chain as in our earlier polymer density functional theory study.[29] The simulation for CO_2 involved the total of 1000 particles, whereas that of C_{28} used 140 chains.

In evaluating the solubility of CO_2 in polymer, we again used the Gibbs ensemble simulation. CO_2 molecules were allowed to move between two boxes, one representing the pure CO_2 gas phase and the other being the polymer-CO_2 liquid mixture. In contrast, polymer molecules were confined to the liquid phase. The pressure of the two boxes were maintained at a common value by trial volume moves performed separately in each box. The simulation was carried out using the total of 600 CO_2 molecules and 60 C_{28} chains.

Table 1 lists the resulting Lennard–Jones parameter in reduced units in which ϵ_{pp} and σ_{pp} are both unity. The table also lists their values in physical units after making necessary conversions using the critical temperature (844 K) and pressure (0.954 MPa) for C_{28}.

Thermodynamic properties

To evaluate the relevant interfacial properties, we used a rectangular simulation box under periodic boundary conditions with its height $80\sigma_{pp}$ and its cross section being a square of length $20\sigma_{pp}$. The system was closed to polymer chain but was open to CO_2 molecules. Thus, CO_2 molecules were subjected to grand canonical Monte Carlo moves at several values of the absolute fugacity (0.01—0.05 in reduced units) resulting in the pressure values approximately between 1 and 5 MPa. The system temperature was held at $k_BT/\epsilon_{pp}=$ 0.8178681, 0.8431774, and 0.8684866 corresponding to 323.15, 333.15, and 343.15 K, respectively.

To explore the effect of the chain length, we considered three cases $n=10$, 20, and 40 without any change in the other model parameters. The number of polymer segments in the system was fixed at 8000, resulting in the film thickness between $20\sigma_{pp}$ and $23\sigma_{pp}$ in all cases we considered. This was deemed sufficient to eliminate artificial film thickness dependence based on our prior polymer density functional study.[29] However, the systems with longer chains are expected to be less efficient in exploring representative statistical states. Accordingly, we will often report only on the results for $n=10$ unless the n dependence is at the center of discussion.

The formulae for γ_∞ and z_s were taken from the literature[12,13,30] and are elaborated in Appendix D.

To evaluate the bulk properties, we also performed Gibbs ensemble simulation with 1000 polymer segments. The usual moves to exchange gas particles between the two boxes and also the trial repartitioning of the (fixed) total volume between the boxes ensured the equality of the CO_2 chemical potential and the pressure between the two phases. In addition, the gas phase was subjected to grand canonical moves with the same fugacity values used in the interface simulations. From the simulation, we obtained p^β, v^β, and x_g. To evaluate V_i^α, we measured the volume of the mixture as a function of the number of CO_2 molecules it contained and fit the result to a line, the slope of which is V_g^α. Then, V_p^α is

Table 1. Lennard–Jones Parameters for Simulation

ij	σ_{ij}^*	ϵ_{ij}^*	σ_{ij}(Å)	ϵ_{ij}(J)
gg	0.9676	0.7177	3.674	3.915×10^{-21}
gp	0.9828	0.8069	3.735	4.402×10^{-21}
pp	1	1	3.797	5.455×10^{-21}

The starred quantities are in reduced units in which ϵ_{pp} and σ_{pp} are unity.

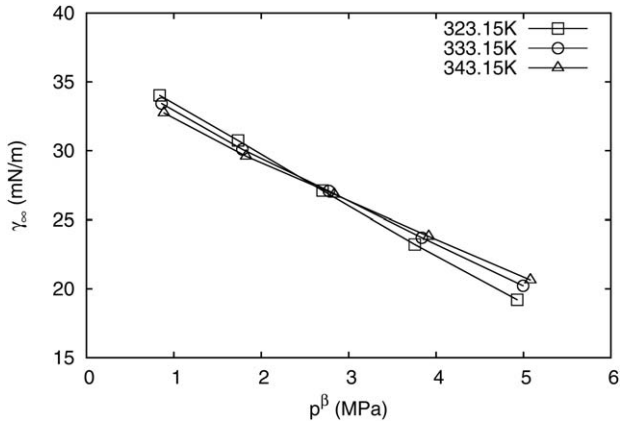

Figure 3. Effects of T and p^β on γ_∞ of C_{28} ($n = 10$).

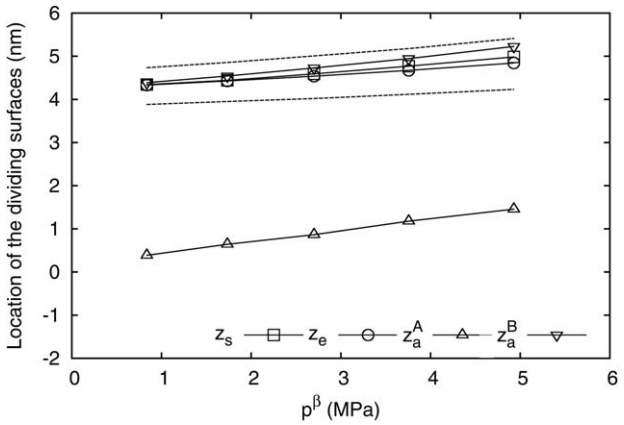

Figure 4. Location of the dividing surfaces measured from the center of the liquid mixture toward the vapor phase.

***T*=323.15K and $n = 10$. The dashed lines mark the interfacial region in which the polymer density is between 5 and 95% of the bulk liquid-phase value.**

obtained from the identity $v^\alpha = x_g V_g^\alpha + x_p V_p^\alpha$, where v^α is the molar volume of the mixture.

As explained in Appendix B, both z_a and z_e were determined by combining the results of interface simulations and the Gibbs ensemble simulation just described.

Results

Figure 3 shows the dependence of γ_∞ on p^β. We observe that γ_∞ decreases with p^β. From Eq. 3, we conclude that $\Gamma_{g,e} > 0$, that is, the surface adsorption of CO_2 is positive when referred to the equimolar dividing surface for the polymer. In fact, in all cases we studied, density profiles across the interface show a marked increase of CO_2 density in the interfacial region compared to the bulk values. Figure 3 also shows an interesting crossover behavior, that is, γ_∞ decreases with increasing T at lower values of p^β but the trend reverses at higher p^β. This behavior was also observed for $n = 20$ and 40, and is consistent with the findings of both experimental and theoretical studies[31,32] including the predictions of polymer density functional theory by Talreja,[33,34] who offered the first mechanistic interpretation of the crossover behavior. Here, we note the following identity which can be derived from Eqs. A5 and B1

$$\left(\frac{\partial \gamma_\infty}{\partial T}\right)_{p^\beta} = s^\beta \Gamma_{g,e} - s_e^s \tag{27}$$

where s^β is the entropy of the gas phase defined on the per molecule basis and s_e^s is the superficial entropy per unit area of the equimolar dividing surface. For low enough p^β, $\Gamma_{g,e}$ is sufficiently small and the second term dominates. Insofar as s_e^s is expected to be positive, $(\partial \gamma_\infty / \partial T)_{p^\beta}$ is negative. However, the observed reversal in the sign of the partial derivative indicates that, when $\Gamma_{g,e}$ increases with p^β, the first term starts to dominate even though s^β decreases at the same time.

Because $\Gamma_{g,e}$ increases more rapidly at lower temperatures, the crossover behavior was seen to disappear when we plot γ_∞ against $\Gamma_{g,e}$. Likewise, there was no crossover behavior in γ_∞ vs x_g plot at least over the range of conditions we explored. However, the derivative $\partial \gamma_\infty / \partial T$ is most easily evaluated when p^β, rather than x_g or $\Gamma_{g,e}$, is held fixed.

Figure 4 shows the location of the various dividing surfaces for the case of $n = 10$ at 323.15 K. The distance is measured from the center of the liquid film defined as the plane parallel to the interface and passing through the center of mass of the entire collection of the polymer segments. As expected, the surface of tension (z_s) and equimolar dividing surface (z_e) are both situated within the interfacial region. Because the auxiliary surface z_a^B for path B as defined by Eq. 10 is located very close to z_s and z_e, the approximate relation Eq. 14 is untenable at least under the conditions explored here. In contrast, the auxiliary surface z_a^A for path A as defined by Eq. 9 is located deep inside the liquid film. Thus, we expect Eq. 13 to yield a reasonably accurate estimate of δ_∞^A. According to the convention noted below Eq. 11, $\delta_\infty^A > 0$.

Within the parameter values we explored, z_s, z_e, and z_a^B are all found to be insensitive to n and T. Figure 5 illustrates this for z_s. The figure also shows that z_a^A is insensitive to n. However, the effect on z_a^A of raising T by 20 K is clearly noticeable.

The resulting values of the Tolman length, δ_∞^A, for path A are shown in Figure 6. The approximate values of δ_∞^A due to Eq. 13 are shown in Figure 7 and seen to be in excellent agreement with the exact values. We recall that p^β at saturation for path A is identified with the final pressure p_f at

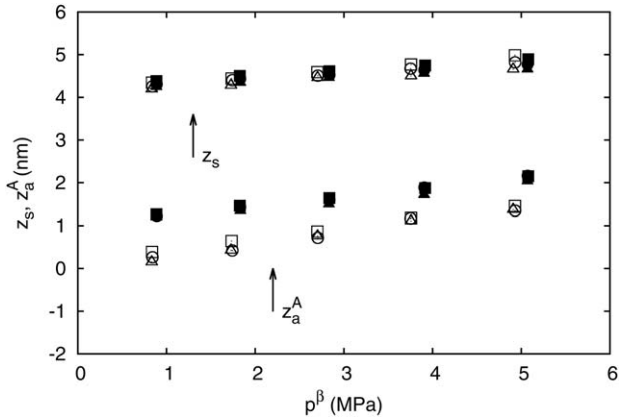

Figure 5. Location of the dividing surfaces z_s and z_a^A.

Squares, circles, and triangles are, respectively, data for $n = 10$, 20, and 40. The open symbols represent data at 323.15 K and the filled ones are data at 343.15 K.

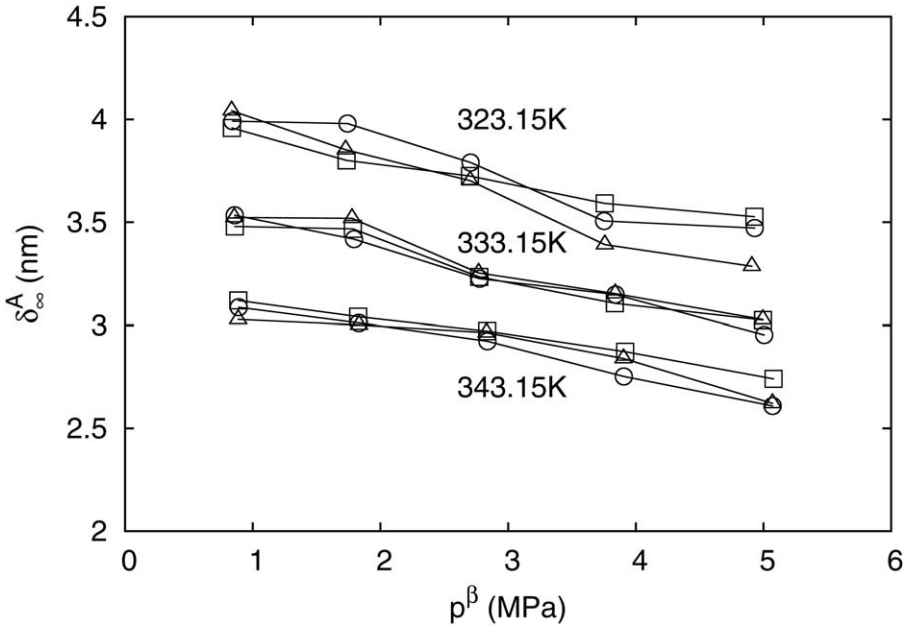

Figure 6. Dependence of δ_∞^A on T, p^β, and n.

Data for $n = 10$, 20, and 40 are represented, respectively, by squares, circles, and triangles.

which foaming takes place, which is in the range being considered here.

As a result of the aforementioned rather weak n dependence of z_s and z_a^A, δ_∞^A also depends rather weakly on n as seen clearly in Figures 6 and 7. This trend can be easily understood from the approximate Eq. 13. As noted in our polymer density functional study,[29,33] $\Gamma_{g,e}$ is a linear function of n^{-1} with rather weak dependence on n^{-1}. When n changes from 10 to 40, for example, $\Gamma_{g,e}$ changes only by about 3%. On the other hand, v^β is determined solely by T and p^β and is independent of n, thus, leading to the observed weak n dependence of δ_∞^A. Importantly, this also implies that Eq. 13 remains valid when n is increased to reach the values typical of actual polymers.

Figures 6 and 7 exhibit a weak dependence of δ_∞^A on p^β. In view of Eq. 13, this implies that a γ_∞ vs. p^β plot is slightly concave up, a conclusion consistent with the results in Figure 3 as well as with our previous polymer density functional studies.[29,33]

Because z_s and z_a^B both lie within the interfacial region, δ_∞^B is considerably smaller compared to δ_∞^A and the approximation Eq. 14 is not valid. Nevertheless, Eq. 14 does capture the qualitative trends rather well as illustrated in Figure 8.

It is important to keep in mind that p^β relevant for path B is identified with p_i and is much larger than what we used in our simulation. However, the interfacial simulation under such conditions requires considerably larger number of particles (both CO_2 and polymer segments) to realize bulk-like properties toward the center of the film. As a result, we have not been able to perform a comprehensive simulation study at higher p^β values. Thus, our remarks on δ_∞^B given here is only tentative, prompting for a further study. As z_s and z_a^B are comparable in magnitude, it may prove important to investigate systematically the system size dependence of δ_∞^B. This is indeed the case at least with single-component systems, in which the Tolman length is given by $z_e - z_s$ and is considerably smaller in magnitude than the particle diameter.[13,14]

An estimate of λ

Because a sharply defined onset of the spinodal is an artifact of a mean-field theory, it is not straightforward to determine the onset by simulation. Nevertheless, it will be of interest to estimate λ and predict the dependence of ψ (or $\phi = \psi^3$) on η and we report on our findings of our (limited) effort in this direction.

To obtain a rough estimate of Δp_{sp} for path A, we used a variant of Gibbs ensemble simulation, in which two simulation boxes, one containing pure CO_2 gas phase and the other containing the polymer-CO_2 mixture, are held at the same temperature but at different pressures. To ensure the equality of chemical potential of CO_2, CO_2 molecules are exchanged between the boxes as in the usual Gibbs ensemble simulation. When the gas-phase pressure p^β is increased while maintaining T and the pressure p^α of the mixture constant, CO_2 mole fraction x_g in the mixture was found to increase suddenly over a very small interval of p^β.

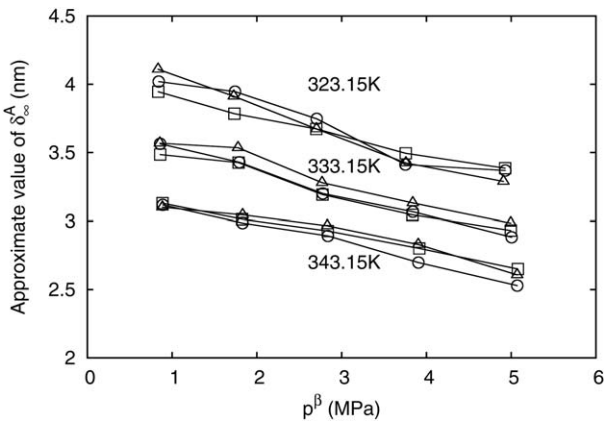

Figure 7. Approximate values of δ_∞^A by means of Eq. 13.

The symbols are the same as in Figure 6.

We recall that the onset of the mean-field spinodal is identified with an extremum of μ_g^α, that is, $(\partial\mu_g^\alpha/\partial x_g)_{T,p^\alpha}=0$ at the onset. Thus, when x_g is viewed as a function of μ_g^α, which increases monotonically with p^β [because $\mu_g^\alpha=\mu_g^\beta$ and $(\partial\mu_g^\beta/\partial p^\beta)_T=v^\beta>0$], we expect that x_g increases rapidly when p^β approaches the value at the onset. In practice, the extremum is very difficult to locate precisely because the mixture phase readily undergoes phase separation when the free energy barrier of bubble nucleation becomes comparable with k_BT. Nevertheless, because the increase of x_g occurs over a narrow range of p^β, a value of $p^\beta-p^\alpha$ taken from this range of p^β serves as a fairly accurate estimate of Δp_{sp} at given T and p^α.

For $n=10$ at 323.15 K and 0.836 MPa, this procedure yielded $\Delta p_{sp}\approx 8$ MPa, which is in fair agreement with another estimate, $\Delta p_{sp}=8.5$ MPa, by a version of polymer density functional theory[29] when the model parameters in the theory were adjusted to reproduce experimentally determined critical temperature and pressure of pure phases (CO_2 and C_{28}) as well as CO_2 solubility (at $T=323.15$ K and pressure up to 5 MPa) from Gibbs ensemble simulations. Using $\gamma_\infty=34.02$ mN/m, $\delta_\infty^A=3.958$nm (exact), and $\delta_\infty^A=3.946$nm (approximate) at 323.15 K and 0.836 MPa for $n=10$, we found $\eta_{sp}=0.931$ (exact) and $\eta_{sp}=0.930$ (approximate), for which λ is 0.445 and 0.443, respectively. Using these values of λ in Eq. 24, we computed φ as a function of the normalized degree of supersaturation η/η_{sp}. These two values of λ yield nearly identical φ vs. η/η_{sp} plots and Figure 9 includes the result only for $\lambda=0.445$ along with those for rather different values of λ.

That these curves being concave up is in agreement with a self-consistent field theory calculation for bubble nucleation in a model system of CO_2-hexadecane binary mixture.[35] Equation 23 indicates that, for a positive value of λ, δ vanishes as the mean-field spinodal is approached. As noted below Eq. C5, $\partial\phi/\partial\eta$ also vanishes at the onset of the mean-field spinodal in this case, a conclusion consistent with Figure 9. However, $\partial\psi/\partial\eta$ is $-\infty$ for $\lambda<2/3$. This divergent behavior of ψ (or γ) is also observed in the case of a single-component system.[36]

The figure also includes the ϕ vs. η/η_{sp} plot at three additional values of λ. We observed that, at a given value of η/η_{sp}, ϕ decreases with increasing λ. (Because η_{sp} increases with λ, however, if we plot ϕ against η, then, ϕ is seen to increases

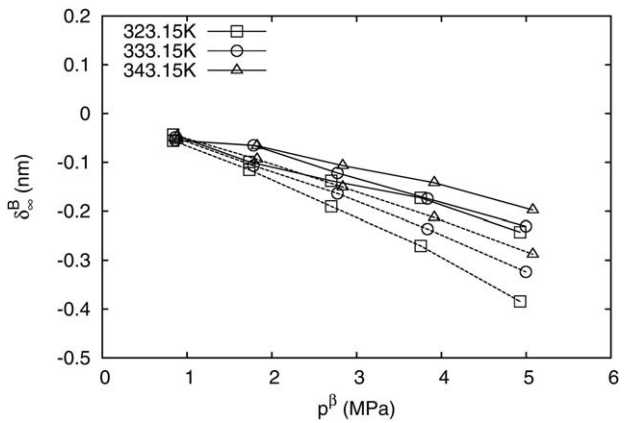

Figure 8. Approximate values of δ_∞^B by means of Eq. 14.

The solid lines show δ_∞^B for $n=10$. Each dashed line shows the approximate values based on Eq. 14 and corresponds to the solid line with the same symbol.

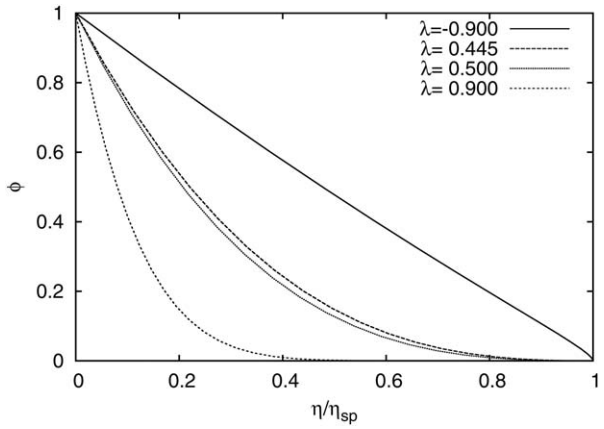

Figure 9. Dependence of φ on the normalized degree of supersaturation η/η_{sp} for various values of λ between −0.9 and 0.9.

with increasing λ for a given value of η.) We note that the plot for $\lambda=0.5$ is essentially identical to those corresponding to other two values of λ, 0.445 and 0.443. From what was said earlier, the usual Tolman correction, Eq. 18, is seen to be accurate under the particular condition we examined here, provided that the ansatz Eq. 23 is appropriate. This conclusion, however, should not be generalized without a more systematic study covering a much wider range of conditions. In fact, ϕ for $\lambda=\pm 0.9$ are considerably different from those for $\lambda\approx 0.5$. Finally, consistent with the observation made in Appendix C, $\partial\phi/\partial\eta$ at the onset ($\eta/\eta_{sp}=1$) is $-\infty$ when $\lambda=-0.9$, although the divergent behavior becomes detectable only extremely close to the onset.

Summary

We developed an approximation scheme to estimate the Tolman length δ_∞ at the low supersaturation regime in the case of bubble nucleation in polymer-gas mixtures.

The approximation requires, as inputs, macroscopic thermodynamic properties only. The accuracy of the approximation was examined by comparing against simulations performed on a simple model system of polymer-CO_2 mixtures. We recall that the binary system permits two distinct modes of analyzing a set of nucleation experiments performed at various values of pressure and gas species mole fraction. This lead to two distinct approximate formula for δ_∞, Eqs. 13 and 14.

At the pressure values relevant to path A, the approximation proves accurate. In contrast, the required computational effort prevented us from examining the approximation scheme for path B under the pressure values most relevant for that path. At lower pressure values, the approximation for path B is untenable. It is of great interest to perform a more thorough analysis of path B under much higher pressure values than those we considered here. We expect that polymer density functional theory will provide us with a viable option that is less demanding computationally.

At least for path A then, δ_∞ can be estimated from readily accessible thermodynamic properties. From this follows the Tolman correction to the free energy barrier W of nucleation, Eq. 20. The correction, however, is applicable only at the low supersaturation regime. In an attempt to estimate W over the entire range of supersaturation without resorting to molecular theories, we introduced a simple ansatz, Eq. 23, for

the supersaturation dependence of δ. In this way, we obtained W with correct thermodynamic behavior both in the low supersaturation regime and at the onset of the spinodal. Because the onset can be determined from the equation of state of the polymer-gas mixture, our approach, in principle, requires macroscopically accessible information only. In this sense, it may be considered as a logical extension of classical theory with built in thermodynamic consistency. Of course, the usefulness of the approach should not be overstated. In particular, the accuracy of Eq. 23 is subject to verification either by means of bubble nucleation experiments or microscopic theories. Nevertheless, our approach should represent a vast improvement over classical theory, according to which $\psi \equiv \phi \equiv 1$.

Acknowledgments

This work was supported by the National Science Foundation (CMMI-0620911). Computations reported here were made possible by a resource grant from the Ohio Supercomputer Center.

Literature Cited

1. Shafi MA, Joshi K, Flumerfelt RW. Bubble size distributions in freely expanded polymer foams. *Chem Eng Sci*. 1997;52:635–644.
2. Joshi K, Lee JG, Shafi MA, Flumerfelt RW. Prediction of cellular structure in free expansion of viscoelastic media. *J Appl Polym Sci*. 1998;67:1353–1368.
3. Tomasko DL, Burley AC, Feng L, Yeh SK, Miyazono K, Nirmal-Kumar S, Kusaka I, Koelling K. Development of CO_2 for polymer foam applications. *J Supercrit Fluids*. 2009;47:493–499.
4. Zettlemoyer AC, ed. Nucleation. New York: Marcel Dekker, 1969.
5. Tolman RC. Consideration of the Gibbs theory of surface tension. *J Chem Phys*. 1948;16:758–774.
6. Tolman RC. The superficial density of matter at a liquid-vapor boundary. *J Chem Phys*. 1949;17:118–127.
7. Tolman RC. The effect of droplet size on surface tension. *J Chem Phys*. 1949;17:333–337.
8. Koenig FO. On the thermodynamic relation between surface tension and curvature. *J Chem Phys*. 1950;18:449–459.
9. Falls AH, Scriven LE, Davis HT. Structure and stress in spherical microclusters. *J Chem Phys*. 1981;75:3986–4002.
10. Nishioka K, Tomino H, Kusaka I, Takai T. Curvature dependence of the interfacial tension in binary nucleation. *Phys Rev A*. 1989;39:772–782.
11. Tomino H, Kusaka I, Nishioka K, Takai T. Interfacial tension for small nuclei in binary nucleation. *J Cryst Growth*. 1991;113:633–636.
12. van Giessena AE, Blokhuis EM. Determination of curvature corrections to the surface tension of a liquid-vapor interface through molecular dynamics simulations. *J Chem Phys*. 2002;116:302–310.
13. Lei YA, Bykov T, Yoo S, Zeng XC. The Tolman length: is it positive or negative? *J Am Chem Soc*. 2005;127:15346–15347.
14. van Giessena AE, Blokhuis EM. Direct determination of the Tolman length from the bulk pressures of liquid drops via molecular dynamics simulations. *J Chem Phys*. 2009;131:164705–1–164705–9.
15. Barrett J. First-order correction to classical nucleation theory: a density functional approach. *J Chem Phys*. 1999;111:5938–5946.
16. Xue YQ, Yang XC, Cui ZX, Lai WP. The effect of microdroplet size on the surface tension and Tolman length. *J Phys Chem B*. 2011;115:109–112.
17. Gibbs JW. The Scientific Papers of J. Willard Gibbs, Vol. I. Thermodynamics, Woodbridge, Connecticut: Ox Bow Press;1993:252–258.
18. Nishioka K. Thermodynamic formalism for a liquid microcluster in vapor. *Phys Rev A*. 1987;36:4845–4851.
19. Li H, Lee LJ, Tomasko DL. Effect of CO_2 on the interfacial tension of polymer melts. *Ind Eng Chem Res*. 2004;43:509–514.
20. Shen VK, Debenedetti PG. Density-functional study of homogeneous bubble nucleation in the stretched Lennard-Jones fluid. *J Chem Phys*. 2001;114:4149–4159.
21. Kusaka I. On the scaling behavior of the free energetics of nucleation. *J Chem Phys*. 2003;118:5510–5515.
22. Gibbs JW. The Scientific Papers of J. Willard Gibbs, Vol. I. Thermodynamics, Woodbridge, Connecticut: Ox Bow Press; 1993:226–227.
23. Talanquer V. A new phenomenological approach to gas-liquid nucleation based on the scaling properties of the critical nucleus. *J Chem Phys*. 1997;106:9957–9960.
24. Kashchiev D. Thermodynamically consistent description of the work to form a nucleus of any size. *J Chem Phys*. 2003;118:1837–1851.
25. Kusaka I. A scaling function of nucleation barrier based on the diffuse interface theory. *J Chem Phys*. 2003;119:1808–1812.
26. Press WH, Teukolsky SA, Vetterling WT, Flannery BP. Numerical Recipes. Cambridge: Cambridge University Press, 1992.
27. Frenkel D, Smit B. Understanding Molecular Simulation, 2nd ed. San Diego: Academic Press, 2002.
28. Sato Y, Tagashira Y, Maruyama D, Takishima S, Masuoka H. Solubility of carbon dioxide in eicosane, docosane, tetracosane, and octacosane at temperatures from 323 to 473 K and pressures up to 40 MPa. *Fluid Phase Equilib*. 1998;147:181–193.
29. Talreja M, Kusaka I, Tomasko DL. Density functional approach for modeling CO_2 pressurized polymer thin films in equilibrium. *J Chem Phys*. 2009;130:084902-1–084902-11.
30. Haye MJ, Bruin C. Molecular dynamics study of the curvature correction to the surface tension. *J Chem Phys*. 1994;100:556–559.
31. Mejía A, Polishuk I, Segura H, Wisniak J. Estimation of interfacial behavior using the global phase diagram approach I. Carbon dieside– n-alkanes. *Thermochimica Acta*. 2004;411:171–176.
32. Li Z, Firoozabadi A. Interfacial tension of nonassociating pure substances and binary mixtures by density functional theory combined with Peng-Robinson equation of state. *J Chem Phys*. 2009;130:154108-1–154108-9.
33. Talreja M. Towards understanding interfacial phenomena in polymer-CO_2 systems. Ph.D. thesis, The Ohio State University, 2010. http://etd.ohiolink.edu/view.cgi?acc_num=osu1275007561.
34. Talreja M, Kusaka I, Tomasko DL. Analyzing surface tension in higher alkane and their CO_2 mixtures. *Fluid Phase Equilibria*. 2012:67–76.
35. Müller M, MacDowell LG, Virnau P, Binder K. Interface properties and bubble nucleation in compressible mixtures containing polymers. *J Chem Phys*. 2002;117:5480–5496.
36. Corti DS, Kerr KJ, Torabi K. On the interfacial thermodynamics of nanoscale droplets and bubbles. *J Chem Phys*. 2011;135:024701–1–024701–20.
37. Gibbs JW. The Scientific Papers of J. Willard Gibbs, Vol. I. Thermodynamics, Woodbridge, Connecticut: Ox Bow Press;1993: 229–231.

Appendix A: GTK Equation

More than 60 years ago, Tolman[5–7] considered the supersaturation dependence of W and derived an expression for $\partial \ln \gamma / \partial q$ in a single-component system. His result was immediately generalized by Koenig[8] to multicomponent systems. Although the latter formulation is extremely general to embrace the specific case that concerns us in this work, it appears beneficial to trace his formulation within the much simpler context of bubble nucleation in a binary polymer-gas mixture. For simplicity, we will also set the polymer concentration in bulk β phase identically to zero.

We emphasize that our thermodynamic analysis pertains only to a critical nucleus which is in (unstable) equilibrium with the metastable phase. As a result, infinitesimal changes in the intensive state of the metastable phase we shall consider in what follows is accompanied by the corresponding change in the state of the critical nucleus that must take place to maintain that equilibrium.

To conform to the GTK formalism, we first change our independent variables from Δp occurring in Eqs. 6 and 7 to q. For this purpose, Eq. 15 is differentiated to yield

$$d\Delta p = 2\gamma\left(1 + q\frac{\partial \ln \gamma}{\partial q}\right)dq \tag{A1}$$

where, as discussed in the main text, the variables held fixed in the partial derivative depend on the path being taken. Using Eq. A1, we find that

$$\frac{\partial\psi}{\partial\Delta p}=\frac{1}{\gamma_\infty}\frac{\partial\gamma}{\partial\Delta p}=\frac{1}{2\gamma_\infty}\frac{\partial\ln\gamma/\partial q}{1+q\partial\ln\gamma/\partial q} \tag{A2}$$

The starting point of Koenig's derivation is the Gibbs adsorption equation applied for a spherical interface and written in reference to the surface of tension[37]

$$d\gamma=-s^s dT-\Gamma_g d\mu_g-\Gamma_p d\mu_p \tag{A3}$$

where μ_p is the chemical potential of the polymer, s^s is the superficial entropy, and Γ_i is the excess number of molecules of species i, all attributed to the unit area of the dividing surface. Our convention for Γ_i means that μ_i is on a per molecule basis. Because we are concerned only with the critical nucleus, for which Eq. 3 holds, we dropped the superscripts from μ_g even though the form of the function μ_g^α differs from that of μ_g^β in general. We also require the Gibbs–Duhem relation for the bulk phase α

$$s^\alpha dT-v^\alpha dp^\alpha+x_g d\mu_g+x_p d\mu_p=0 \tag{A4}$$

and bulk phase β

$$s^\beta dT-v^\beta dp^\beta+d\mu_g=0 \tag{A5}$$

in which s^i and v^i denote, respectively, the entropy and the volume in phase i defined on the per molecule basis, and x_p is the mole fraction of the polymer.

Path A

Our independent variables are now

$$(T,p^\alpha,q) \tag{A6}$$

in place of those listed in Eq. 6. From Eq. A3, we find

$$\left(\frac{\partial\gamma}{\partial q}\right)_{T,p^\alpha}=-\Gamma_g\left(\frac{\partial\mu_g}{\partial q}\right)_{T,p^\alpha}-\Gamma_p\left(\frac{\partial\mu_p}{\partial q}\right)_{T,p^\alpha} \tag{A7}$$

where the change in q at fixed T and p^α is physically brought about through the change in p_i and hence that in x_g.

The partial derivatives occurring on the right hand side of Eq. A7 can be evaluated as follows. From Eq. A5

$$\left(\frac{\partial\mu_g}{\partial q}\right)_{T,p^\alpha}=v^\beta\left(\frac{\partial p^\beta}{\partial q}\right)_{T,p^\alpha} \tag{A8}$$

which may be combined with Eq. A4 to give

$$\left(\frac{\partial\mu_p}{\partial q}\right)_{T,p^\alpha}=-\frac{x_g}{x_p}\left(\frac{\partial\mu_g}{\partial q}\right)_{T,p^\alpha}=-\frac{x_g v^\beta}{x_p}\left(\frac{\partial p^\beta}{\partial q}\right)_{T,p^\alpha} \tag{A9}$$

Differentiating Eq. 15 with respect to q, or directly from Eq. A1, we obtain

$$\left(\frac{\partial p^\beta}{\partial q}\right)_{T,p^\alpha}=2\gamma\left[1+q\left(\frac{\partial\ln\gamma}{\partial q}\right)_{T,p^\alpha}\right] \tag{A10}$$

Combining Eqs. A7, A8, A9, and A10, we obtain

$$\left(\frac{\partial\ln\gamma}{\partial q}\right)_{T,p^\alpha}=\frac{\frac{2v^\beta}{x_p}\left(x_g\Gamma_p-x_p\Gamma_g\right)}{1-\frac{2v^\beta}{x_p}\left(x_g\Gamma_p-x_p\Gamma_g\right)q} \tag{A11}$$

Let R_a denote the radius of the auxiliary surface for which Eq. 9 holds. We note that the total number of gas molecules N_g contained in the system of volume V, which is consisting of a single critical nucleus and the surrounding metastable phase α, may be expressed as

$$\begin{aligned}N_g&=\frac{4\pi}{3}R^3\rho_g^\beta+\left(V-\frac{4\pi}{3}R^3\right)\rho_g^\alpha+4\pi R^2\Gamma_g\\&=\frac{4\pi}{3}R_a^3\rho_g^\beta+\left(V-\frac{4\pi}{3}R_a^3\right)\rho_g^\alpha+4\pi R_a^2\Gamma_{g,a}\end{aligned} \tag{A12}$$

where ρ_g^i is the number density of gas molecules in phase i. Now, let

$$\delta:=R_a-R \tag{A13}$$

denote the distance between the two dividing surfaces. Equation A12 then yields

$$\Gamma_g=(1+\delta q)^2\Gamma_{g,a}-\delta\left(1+\delta q+\frac{1}{3}\delta^2q^2\right)\left(\rho_g^\alpha-\rho_g^\beta\right) \tag{A14}$$

Replacing the subscript g by p in Eq. A14 and noting that $\rho_p^\beta\equiv 0$, we obtain

$$\Gamma_p=(1+\delta q)^2\Gamma_{p,a}-\delta\left(1+\delta q+\frac{1}{3}\delta^2q^2\right)\rho_p^\alpha \tag{A15}$$

where ρ_p^α is the number density of polymer molecules in phase α. Using Eqs. A14 and A15 as well as the identity

$$x_g\rho_p^\alpha-x_p\left(\rho_g^\alpha-\rho_g^\beta\right)\equiv\frac{x_p}{v^\beta} \tag{A16}$$

where we note that $\rho_g^\beta=1/v^\beta$, we may express the right hand side of Eq. A11 in terms of δ. The final result is

$$\left(\frac{\partial\ln\gamma}{\partial q}\right)_{T,p^\alpha}=-\frac{2\delta\left(1+\delta q+\frac{1}{3}\delta^2q^2\right)}{1+2\delta q\left(1+\delta q+\frac{1}{3}\delta^2q^2\right)} \tag{A17}$$

which is known as the GTK equation.

From Eqs. A2 and A17, we find

$$\left(\frac{\partial\psi}{\partial\Delta p}\right)_{T,p^\alpha}=-\frac{\delta}{\gamma_\infty}\left(1+\delta q+\frac{1}{3}\delta^2q^2\right) \tag{A18}$$

which is Eq. 8 written for path *A*.

Path B

In this case, we use

$$(T,q,x_g) \tag{A19}$$

as the independent variables. Then, in place of Eq. A7, we have

$$\left(\frac{\partial\gamma}{\partial q}\right)_{T,x_g}=-\Gamma_g\left(\frac{\partial\mu_g}{\partial q}\right)_{T,x_g}-\Gamma_p\left(\frac{\partial\mu_p}{\partial q}\right)_{T,x_g} \tag{A20}$$

We note that, when T and x_g are held fixed, there is a one to one correspondence between q and p^α and that the change in q is induced physically by changing p^α. From $\mu_i=\mu_i\left(T,p^\alpha,x_g\right)$ for the mixture, we obtain

$$\left(\frac{\partial\mu_i}{\partial q}\right)_{T,x_g}=\left(\frac{\partial\mu_i}{\partial p^\alpha}\right)_{T,x_g}\left(\frac{\partial p^\alpha}{\partial q}\right)_{T,x_g}=V_i^\alpha\left(\frac{\partial p^\alpha}{\partial q}\right)_{T,x_g} \tag{A21}$$

where V_i^α is the partial molar volume of species i in phase α and we used one of the Maxwell relations. Furthermore, we obtain from Eq. 15

$$\left(\frac{\partial p^{\alpha}}{\partial q}\right)_{T,x_g} = \frac{2}{Z}\left[\gamma + q\left(\frac{\partial \gamma}{\partial q}\right)_{T,x_g}\right] \tag{A22}$$

where

$$Z := \left(\frac{\partial p^{\beta}}{\partial p^{\alpha}}\right)_{T,x_g} - 1 = \frac{V_g^{\alpha}}{v^{\beta}} - 1 \tag{A23}$$

The last equality follows from Eq. 3. Combining Eqs. A20, A21, and A22, we obtain

$$\left(\frac{\partial \ln \gamma}{\partial q}\right)_{T,x_g} = -\frac{2\left(V_g^{\alpha}\Gamma_g + V_p^{\alpha}\Gamma_p\right)}{Z + 2q\left(V_g^{\alpha}\Gamma_g + V_p^{\alpha}\Gamma_p\right)} \tag{A24}$$

From this equation and the identity

$$V_g^{\alpha}\left(\rho_g^{\alpha} - \rho_g^{\beta}\right) + V_p^{\alpha}\rho_p^{\alpha} = -Z \tag{A25}$$

it is now straightforward to show that Eqs. A17 and A18 hold as they are just by replacing p^{α} by x_g in the list of variables being fixed provided that the auxiliary surface is now defined by Eq. 10.

Appendix B: Derivation of Eqs. 13 and 14

We first recall the Gibbs adsorption equation written for the equimolar dividing surface

$$d\gamma = -s_e^s dT - \Gamma_{g,e} d\mu_g + C_e dq \tag{B1}$$

where s_e^s and $\Gamma_{g,e}$ are, respectively, the superficial entropy and the surface excess number of gas molecules both defined with respect to a unit area of the equimolar dividing surface. C_e is a function of the intensive state of the metastable phase. For constant, T processes in which saturation is maintained, we have $q \equiv 0$, and hence

$$d\gamma_{\infty} = -\Gamma_{g,e} d\mu_g = -\Gamma_{g,e} v^{\beta} dp^{\beta} \tag{B2}$$

where we used Eq. A5. From Eq. B2, we find

$$\left(\frac{\partial \gamma_{\infty}}{\partial p^{\beta}}\right)_T = -\Gamma_{g,e} v^{\beta} \tag{B3}$$

where the derivative is taken along the saturation line at the given T.

The following relations hold for the system at saturation when it is contained in a box of height $z_{\max}$ and cross-sectional area A

$$\begin{aligned} N_g &= (z_{\max} - z_e)\rho_g^{\alpha} A + z_e \rho_g^{\beta} A + \Gamma_{g,a} A \\ N_p &= (z_{\max} - z_e)\rho_p^{\alpha} A, \end{aligned} \tag{B4}$$

where N_i is the number of molecules of species i in the container. In writing these equations, we place the interface perpendicular to the z axis and put phase α in the region of larger z values. Using z_a as the dividing surface, we obtain

$$\begin{aligned} N_g &= (z_{\max} - z_a)\rho_g^{\alpha} A + z_a \rho_g^{\beta} A + \Gamma_{g,a} A \\ N_p &= (z_{\max} - z_a)\rho_p^{\alpha} A + \Gamma_{p,a} A \end{aligned} \tag{B5}$$

From Eqs. B4 and B5, we find

$$\begin{aligned} \Gamma_{g,a} &= (z_a - z_e)\left(\rho_g^{\alpha} - \rho_g^{\beta}\right) + \Gamma_{g,e} \\ \Gamma_{p,a} &= (z_a - z_e)\rho_p^{\alpha}. \end{aligned} \tag{B6}$$

Combining Eqs. 9, A16, and B6, we arrive at Eq. 13 for path A. If Eq. 10 is used in place of Eq. 9, we arrive at Eq. 14 for path B.

In the interface simulation reported in the main text, $z_{\max}$, A, and N_p were fixed while N_g was determined from the simulation. The various bulk properties were determined from the Gibbs ensemble simulation described in the main text. Then, Eq. 9 or Eq. 10 was solved simultaneously with Eq. B5 to find z_a with a trivial modification to the latter equation to account for the two interfaces present in the system. The second of Eq. B4 was used to determine z_e.

Appendix C: $\lambda<1$

We show that λ appearing in our ansatz Eq. 23 must be less than unity. As we have mentioned a few times, W, γ, and R have to vanish simultaneously at the onset. This is so, because, as W vanishes, Δp determined by Eq. 3 remains finite. Equation 2 implies then that γ must vanish. In light of Eq. 15, however, R must vanish also. But then, Eq. 15 also demands that, at the onset

$$\left.\frac{\partial \gamma}{\partial R}\right|_{sp} = \lim_{R\to 0}\frac{\gamma}{R} = \lim_{R\to 0}\frac{1}{2}\Delta p = \frac{1}{2}\Delta p_{sp} \tag{C1}$$

Rewriting Eq. A17 as

$$\frac{1}{\gamma q}\frac{\partial \gamma}{\partial R} = \frac{2\delta q\left(1 + \delta q + \frac{1}{3}\delta^2 q^2\right)}{1 + 2\delta q\left(1 + \delta q + \frac{1}{3}\delta^2 q^2\right)} \tag{C2}$$

and using Eqs. 15 and C1, we notice that the left hand side approaches unity as the onset of the mean-field spinodal is approached

$$\frac{1}{\gamma q}\frac{\partial \gamma}{\partial R} = \frac{2}{\Delta p}\frac{\partial \gamma}{\partial \mathrm{R}} \to \frac{2}{\Delta p_{sp}}\frac{\Delta p_{sp}}{2} = 1 \tag{C3}$$

in turn implying that

$$\delta q \to \pm\infty \qquad \text{as} \qquad W \to 0 \tag{C4}$$

But, since

$$\delta q = \frac{\delta_{\infty}\Delta p}{2\gamma_{\infty}^{\lambda}}\gamma^{\lambda - 1} \tag{C5}$$

as one can see from Eqs. 15 and 23, λ must be less than unity. For this range of λ, the right hand side of Eq. 24 is dominated by the $\psi^{3\lambda-2}$ term when ψ approaches zero. Thus, the slope $\partial\psi/\partial\eta$ at η_{sp} is zero for $2/3 < \lambda < 1$, a negative number when $\lambda = 2/3$, and $-\infty$ when $\lambda < 2/3$. A similar consideration for $\phi = \psi^3$ indicates that the slope $\partial\phi/\partial\eta$ changes from zero to $-\infty$ with $\lambda = 0$ marking the boundary.

Appendix D: Interfacial Properties

We recall the following formulae for γ_{∞} and $\delta_{\infty} := z_a - z_s$:[12,13,30]

$$\gamma_{\infty} = \int f_1(z')dz' \tag{D1}$$

and

$$\delta_{\infty} = -\frac{1}{\gamma_{\infty}}\int (z' - z_a) f_1(z')dz' - \frac{1}{\gamma_{\infty}}\int f_2(z')dz' \tag{D2}$$

where the functions f_1 and f_2 are given by

$$f_1(z') := \frac{1}{4A}\left\langle \sum_{i\neq j} \frac{dw}{dr_{ij}} \frac{x_{ij}^2+y_{ij}^2-2z_{ij}^2}{r_{ij}} \delta(z'-z_i) \right\rangle \tag{D3}$$

and

$$f_2(z') := \frac{1}{8A}\left\langle \sum_{i\neq j} \frac{dw}{dr_{ij}} \frac{x_{ij}^2+y_{ij}^2-2z_{ij}^2}{r_{ij}} z_{ij}\delta(z'-z_i) \right\rangle \tag{D4}$$

where A is the area of the interface, $\delta(z'-z_i)$ is the Dirac δ-function, $w(r)$ is the interparticle interaction potential and is given either by the truncated and shifted Lennard–Jones potential or the harmonic potential depending on the pair of particles being considered. Finally, $\mathbf{r}_i=(x_i, y_i, z_i)$ is the position vector of the ith particle, $\mathbf{r}_{ij} := \mathbf{r}_j - \mathbf{r}_i$ with components $x_{ij}=x_j-x_i$, $y_{ij}=y_j-y_i$, $z_{ij}=z_j-z_i$, and $r_{ij}=|\mathbf{r}_{ij}|$.

Carrying out the integrals using the explicit expressions for f_1 and f_2, we find

$$\gamma_\infty = \frac{1}{4A}\left\langle \sum_{i\neq j} \frac{dw}{dr_{ij}} \frac{x_{ij}^2+y_{ij}^2-2z_{ij}^2}{r_{ij}} \right\rangle \tag{D5}$$

and

$$z_s = \frac{1}{8A}\left\langle \sum_{i\neq j} \frac{dw}{dr_{ij}} \frac{x_{ij}^2+y_{ij}^2-2z_{ij}^2}{r_{ij}} (z_i+z_j) \right\rangle \tag{D6}$$

In writing Eqs. D1 and D2, one chooses the range of integration to contain both bulk phases and only a single interface in between. As explained in the main text, however, we have a slab of polymer-CO_2 liquid mixture placed in a CO_2 gas phase, and hence there are two interfaces in the system. As far as Eq. D1 is concerned, the integration can be taken along the entire length (in z-direction) of the system provided that the additional factor of $1/2$ is introduced to account for the fact that there are now two interfaces in the system. The same does not hold for Eq. D2. In fact, if we set the origin ($z'=0$) to coincide with the center of mass of the slab, then Eq. D6 would yield $z_s \equiv 0$ for such a choice for the range of integration since the expression is linear in z_i+z_j.

So as to account for a single interface at a time, we computed two estimates for z_s, one resulting from the integration over $0 < z' \leq z_{max}/2$ and the other from the integration over $-z_{max}/2 < z' \leq 0$, where $z_{\max}$ denotes the height of the simulation box as in Eq. B4. The choice for the range of integration in Eq. D2 translates to the restriction on the summation over i in Eq. D6. That is, we need to exclude from the summation over i (but not from that over j) those particles whose z coordinate $z_{\rm i}$ is outside the range of integration, a condition imposed by the δ-function in the defining equations for f_1 and f_2. (The summation over j includes only those particles that are within the cut-off radius from the ith particle.) When the two estimates for δ_∞ were compared, the largest discrepancy was 2.8% of their arithmetic mean for the results reported in this article.

Manuscript received Jun. 11 2012, and revision received Dec. 17, 2012.